High pressure effects on the crystal and magnetic structure of $Pr_{1-x}Sr_xMnO_3$ manganites (x = 0.5–0.56)

2004 J. Phys.: Condens. Matter 16 2381

(http://iopscience.iop.org/0953-8984/16/13/017)

INSTITUTE OF PHYSICS PUBLISHING JOURNAL OF PHYSICS: CONDENSED MATTER

J. Phys.: Condens. Matter **16** (2004) 2381–2394 PII: S0953-8984(04)75064-X

High pressure effects on the crystal and magnetic structure of $Pr_{1-x}Sr_xMnO_3$ manganites (x = 0.5–0.56)

D P Kozlenko[1,2], V P Glazkov[3], Z Jirák[4] and B N Savenko[2]

[1] ISIS Facility, Rutherford Appleton Laboratory, Chilton, Didcot, Oxon OX11 0QX, UK
[2] Frank Laboratory of Neutron Physics, JINR, 141980 Dubna, Moscow Region, Russia
[3] Russian Research Centre 'Kurchatov Institute', 123182 Moscow, Russia
[4] Institute of Physics, Cukrovarnická 10, 162 53 Prague 6, Czech Republic

Received 16 January 2004
Published 19 March 2004
Online at stacks.iop.org/JPhysCM/16/2381 (DOI: 10.1088/0953-8984/16/13/017)

Abstract

The crystal and magnetic structures of the manganites $Pr_{1-x}Sr_xMnO_3$ ($x = 0.5$, 0.56) have been studied by means of powder neutron diffraction at high external pressures up to 4.8 GPa. At ambient pressure both $Pr_{0.44}Sr_{0.56}MnO_3$ and $Pr_{0.5}Sr_{0.5}MnO_3$ have a tetragonal structure (space group $I4/mcm$). At $T_N \approx 215$ K in $Pr_{0.44}Sr_{0.56}MnO_3$ the onset of A-type antiferromagnetic (AFM) state occurs, which is accompanied by a structural phase transformation to the orthorhombic structure (space group $Fmmm$). $Pr_{0.5}Sr_{0.5}MnO_3$ at 175 K $< T < T_C = 265$ K exhibits an intermediate tetragonal ferromagnetic (FM) phase followed by the onset of the orthorhombic A-type AFM phase at $T_N \approx 175$ K. Under high pressure, in $Pr_{0.44}Sr_{0.56}MnO_3$ a tetragonal C-type AFM phase ($T_N \approx 125$ K) appears and the phase separated state is formed, consisting of its mixture with the initial orthorhombic A-type AFM phase ($T_N \approx 220$ K). In $Pr_{0.5}Sr_{0.5}MnO_3$ the application of high pressure leads to a noticeable increase of the FM–A-type AFM transition temperature from $T_N \approx 175$ up to 230 K and formation of a phase separated state below 150 K, consisting of a mixture of orthorhombic A-type AFM phase and tetragonal phase without long range magnetic order. The stability of different magnetic states of $Pr_{0.44}Sr_{0.56}MnO_3$ and $Pr_{0.5}Sr_{0.5}MnO_3$ under high pressure is discussed.

1. Introduction

Manganites of the perovskite type $Ln_{1-x}A_xMnO_3$ (Ln—lanthanum or rare earth, A—alkaline earth elements) exhibit rich magnetic and electronic phase diagrams depending on the kinds of Ln, A elements and their ratio [1]. These systems show for particular compositions an extreme sensitivity of the magnetic, structural, electronic and transport properties to external fields and have attracted considerable interest in relation to the recently discovered colossal magnetoresistance (CMR) effect.

The properties of manganites depend substantially on a balance between the ferromagnetic (FM) interactions mediated by itinerant charge carriers (the double-exchange mechanism [2–4]) and the superexchange interactions between localized spins of manganese ions, which are usually antiferromagnetic (AFM) [5].

The magnetic phase diagrams of manganites with a large average radius of the A-site cation $\langle r_A \rangle$—$La_{1-x}Sr_xMnO_3$ [6], $Pr_{1-x}Sr_xMnO_3$ [6, 7] and to some extent also $Nd_{1-x}Sr_xMnO_3$ [8]—follow over the narrow composition range $0.5 < x < 0.8$ a general trend in the evolution of magnetic ground states: FM metallic $\rightarrow$ A-type AFM metallic $\rightarrow$ C-type AFM insulating state. Each magnetic state possesses characteristic lattice deformation: the tetragonal contraction $c_p/a_p \sim 0.95$ for A-type AFM, elongation $c_p/a_p \sim 1.05$ for C-type AFM and no change from pseudocubic for the FM state. Recent study of thin films of $La_{1-x}Sr_xMnO_3$ grown on substrates with different lattice constants revealed a similar relationship between the induced tetragonal lattice distortion of the manganite and its magnetic order. For $x \sim 0.5$, with the variation of the c_p/a_p lattice parameter ratio of the ideal perovskite cell from 0.97 to 1.06 a change of the magnetic states of $La_{1-x}Sr_xMnO_3$ in the sequence A-type AFM, FM, C-type AFM was found [9]. In a later theoretical study based on first-principles band structure calculations Fang *et al* [10] succeeded in constructing the observed phase diagram of $La_{1-x}Sr_xMnO_3$ manganites taking into account the tetragonal lattice distortion. Such a distortion results in an unlike population of $d(x^2 - y^2)$ and $d(3z^2 - r^2)e_g$ orbitals of Mn ions and in anisotropy of the first-nearest-neighbour exchange integral J_1 along different Mn–O–Mn bonds. The combination of these factors is essential for the stability of the A-type AFM state in the case of $c_p/a_p < 1$ (enhanced population of $d(x^2 - y^2)$ orbitals) and the C-type AFM state in the case of $c_p/a_p > 1$ (enhanced population of $d(3z^2 - r^2)$ orbitals).

The role of lattice distortion in the formation of the phase diagram of doped manganites may be explored directly by structural studies under high external pressure using the neutron diffraction method. It allows one to obtain information on both the pressure-induced lattice distortions of the crystal structure and the related modification of the magnetic structure at a fixed doping level x. Recent structural studies of manganites $La_{0.67}Ca_{0.33}MnO_3$ (FM state at $P = 0$), $Pr_{0.7}Ca_{0.3}MnO_3$ and $Pr_{0.8}Na_{0.2}MnO_3$ (pseudo-CE-type AFM state at $P = 0$) have revealed that application of high pressure results in a noticeable anisotropic distortion of MnO_6 octahedra and leads to the formation of an A-type AFM state in all these compounds [11–13].

For the analysis of the relationship between pressure-induced changes of crystal and magnetic structure in strontium-doped manganites, we have chosen compounds $Pr_{1-x}Sr_xMnO_3$ ($x = 0.5$, 0.56) with similar A-type AFM ground states but different magnetic properties at intermediate temperatures [7, 14, 15]. Both manganites have a tetragonal crystal structure (space group $I4/mcm$) and exhibit a paramagnetic insulating state at ambient conditions. The unit cell of this structure is four times enlarged with respect to the simple perovskite subcell (lattice parameters $a_t \approx a_p\sqrt{2}$ and $c_t \approx 2a_p$). At $P = 0$ and $T_C = 265$ K $Pr_{0.5}Sr_{0.5}MnO_3$ exhibits a transition to a FM metallic state with an orientation of manganese magnetic moments along the c-axis. Below $T_N = 175$ K the A-type AFM metallic state with an orthorhombic structure of $Fmmm$ symmetry (crystallographic cell with $a_o \approx c_o \approx a_t\sqrt{2}$ and $b_o \approx c_t$) develops gradually. The manganese magnetic moments in the magnetic structure of the A-type AFM state (figure 1(a)) are oriented along the b-axis and form ferromagnetic (bc) planes with an antiferromagnetic coupling between them [7, 14]. In the temperature range 135 K $< T <$ 175 K tetragonal FM and orthorhombic A-type AFM phases coexist and at $T <$ 135 K a single A-type AFM phase is observed [14].

The recent study of the magnetic and transport properties of $Pr_{0.5}Sr_{0.5}MnO_3$ performed in the pressure range up to 1.4 GPa reveals that the intermediate tetragonal FM state is destabilized under high pressure [16]. While the Curie temperature changes only slightly

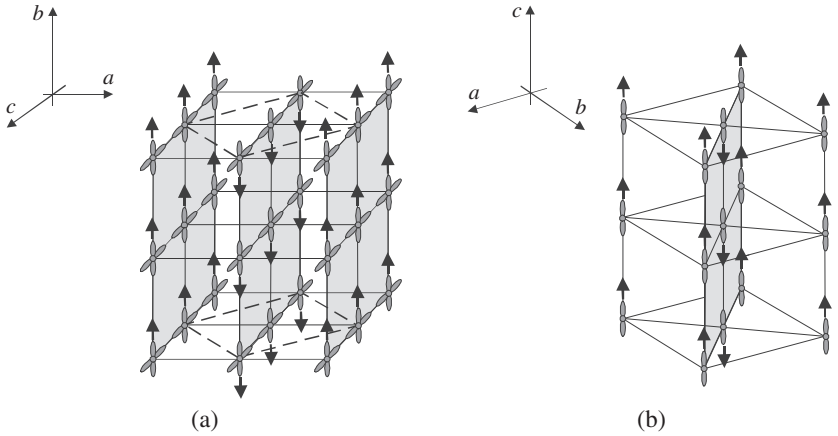

Figure 1. The magnetic structure and e_g orbital polarization in the A-type orthorhombic, space group $Fmmm$, (a) and C-type tetragonal, space group $I4/mcm$, (b) antiferromagnetic phases of $Pr_{1-x}Sr_xMnO_3$. The base of the $I4/mcm$ structure is indicated by dashed lines in the $Fmmm$ structure.

($dT_C/dP = -4$ K GPa^{-1}), the T_N temperature of the transition from the tetragonal FM to the orthorhombic A-type AFM state in $Pr_{0.5}Sr_{0.5}MnO_3$ shows a progressive increase under high pressure, suggesting that the FM tetragonal state might be suppressed fully at the pressure $P \sim 2$ GPa [16].

The second compound, $Pr_{0.44}Sr_{0.56}MnO_3$, does not exhibit the intermediate FM state and at $T_N = 217$ K it directly transforms from the tetragonal paramagnetic to the orthorhombic A-type AFM state through an abrupt first-order structural phase transition [7, 15].

In this paper, the crystal and magnetic structure of $Pr_{0.44}Sr_{0.56}MnO_3$ and $Pr_{0.5}Sr_{0.5}MnO_3$ manganites has been studied by means of powder neutron diffraction at high pressures up to 4.8 GPa in the temperature range 16–290 K.

2. Experimental details

The $Pr_{0.44}Sr_{0.56}MnO_3$ and $Pr_{0.5}Sr_{0.5}MnO_3$ compounds were prepared by solid state reaction at high temperature. Homogenized mixtures of Pr_6O_{11}, $SrCO_3$ and MnO_2 were calcined twice at 950 °C to achieve decarbonation. The powders were then pressed into pellets and heated at 1500 °C in air for 12 h. Afterwards, the sintered samples were slowly cooled to room temperature.

Neutron powder diffraction measurements at ambient pressure and high external pressures up to 4.8 GPa were performed at selected temperatures in the range 16–290 K with the DN-12 spectrometer [17] at the IBR-2 high flux pulsed reactor (FLNP JINR, Dubna, Russia) using sapphire anvil high pressure cells [18]. The sample volume was about 2 mm^3. A special cryostat constructed on the basis of a closed cycle helium refrigerator was used to create a low temperature on the sample.

Several tiny ruby chips were placed at different points of the sample surface. The pressure was determined by the ruby fluorescence technique with the accuracy of 0.05 GPa at each ruby chip and the pressure value on the sample was determined by averaging of values obtained at different points. The estimated inhomogeneity of the pressure distribution on the sample surface was less than 10%.

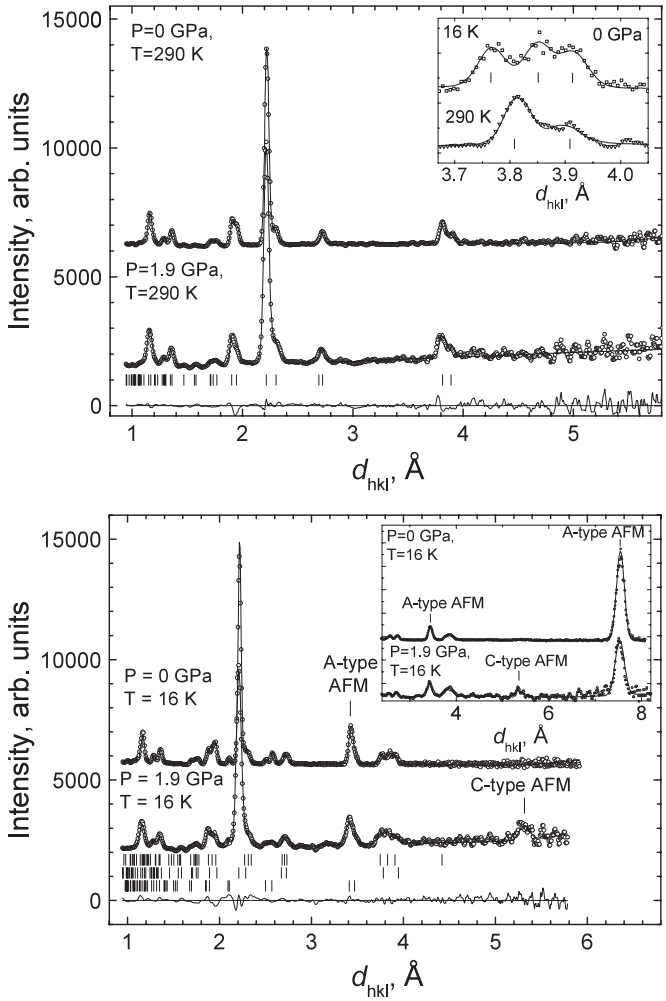

Figure 2. Neutron diffraction patterns of $Pr_{0.44}Sr_{0.56}MnO_3$ measured at $P = 0$ and 1.9 GPa, $T = 290$ and 16 K at scattering angles $2\theta = 90°$ and 45.5° (inset, lower panel) and processed by the Rietveld method. The experimental points, calculated profile and difference curve (for $P = 1.9$ GPa) are shown. Ticks represent the calculated positions of the nuclear peaks of the $I4/mcm$ tetragonal phase in the upper panel and positions of the nuclear (upper row) and magnetic (lower row) peaks of the $Fmmm$ orthorhombic A-type AFM phase and nuclear peaks (middle row) of the $I4/mcm$ tetragonal C-type AFM phase in the lower panel.

Diffraction patterns were collected at scattering angles 45.5° and 90°. The spectrometer resolution at $\lambda = 2$ Å is $\Delta d/d = 0.022$ and 0.015 for these angles, respectively. The typical exposure time at one temperature was 25–30 h. Experimental data were analysed by the Rietveld method using the MRIA program [19], or Fullprof [20] if magnetic structure was to be included.

3. Results

Neutron diffraction patterns of $Pr_{0.44}Sr_{0.56}MnO_3$ obtained at pressures $P = 0$ and 1.9 GPa and $T = 290$ and 16 K are shown in figure 2. At ambient conditions, the tetragonal structure, space group $I4/mcm$, is evidenced. On cooling below $T_N \sim 215$ K, some splitting of diffraction

peaks in the d-spacing regions 1.8–2 and 3.7–3.95 Å (see the inset in the top panel of figure 2) is detected, corresponding to the tetragonal–orthorhombic structural phase transition. In addition, magnetic lines (100) at $d = 7.53$ and (102)/(120) at $d = 3.44$ Å appear, indicating the onset of the A-type AFM state. The structural parameters and the ordered Mn magnetic moments obtained from the Rietveld refinement of the diffraction data for both phases are summarized in table 1. The values of the lattice parameters agree well with ones obtained for single crystals with the close composition $Pr_{0.43}Sr_{0.57}MnO_3$ [7, 15].

Under high pressure $P = 1.9$ GPa, the Néel temperature remains practically unchanged (T_N(A-type) $\sim$ 220 K), but with further temperature decrease, at $T < 125$ K an additional purely magnetic line at $d = 5.4$ Å appears and some other diffraction peaks in the d-spacing region 1.8–2 Å increase notably (figure 2). This observation may be attributed to the onset in $Pr_{0.44}Sr_{0.56}MnO_3$ of the C-type AFM state with a tetragonal structure (space group $I4/mcm$). In the C-type AFM structure (figure 1(b)) manganese spins form ferromagnetic chains along the tetragonal c-axis with an antiferromagnetic coupling between the neighbouring chains. The orthorhombic A-type and tetragonal C-type AFM states coexist down to the lowest temperatures and their calculated fractions at $T = 16$ K are about 77 and 23%, respectively. With pressure increase up to 4.8 GPa, the fraction of C-type AFM state increases up to 30% (see table 1). It is worth mentioning that the C-type AFM structure is the common ground state at ambient pressure in $Pr_{1-x}Sr_xMnO_3$ manganites for higher doping $0.6 < x < 0.9$ [6], and also in $La_{1-x}Sr_xMnO_3$ for $0.65 < x < 0.9$ and $Nd_{1-x}Sr_xMnO_3$ for $0.62 < x < 0.8$ [6, 8].

Neutron diffraction patterns of $Pr_{0.5}Sr_{0.5}MnO_3$ taken at $P = 0$ and 1.9 GPa, $T = 290$, 200 and 16 K are displayed in figure 3. At $P = 0$ and $T < T_C = 265$ K an additional intensity is observed in the two sets of nuclear peaks ((110)/(002)) and ((200)/(112)) of the tetragonal $I4/mcm$ structure which are characteristic of the FM phase. The phase transition to the A-type AFM state with orthorhombic structure of the $Fmmm$ symmetry takes place below $T_N = 175$ K and at $T = 16$ K the single A-type AFM phase is observed. The structural parameters and values of Mn magnetic moments for both tetragonal FM and orthorhombic AFM phases obtained from the Rietveld refinement of the diffraction data at $P = 0$ (table 1) agree well with results of previous studies [14, 15].

Under application of high pressure of $P = 1.9$ GPa, the diffraction patterns of $Pr_{0.5}Sr_{0.5}MnO_3$ change importantly. First, the tetragonal FM and orthorhombic A-type AFM phases coexist at $T = 200$ K and their fractions are determined to be about 35 and 65%, respectively (see table 1). As expected, the FM phase vanishes as temperature is decreased. Nevertheless, the diffraction pattern at 16 K does not correspond to the single $Fmmm$ phase but shows features similar to those found for $Pr_{0.44}Sr_{0.56}MnO_3$ at high pressure and low temperature (figure 2). There is clearly an admixture of the tetragonal $I4/mcm$ phase with a larger distortion, characteristic for the C-type manganites. However, the absence of the magnetic line (100) at $d = 5.4$ Å shows that no ordered Mn magnetic moment related to the C-type AFM state is formed in $Pr_{0.5}Sr_{0.5}MnO_3$. At $P = 1.9$ GPa and $T = 16$ K the calculated fractions of the tetragonal magnetically disordered phase and orthorhombic A-type AFM phase are about 20 and 80%, respectively. With the pressure increase up to 3.2 GPa these values remain nearly the same within an accuracy of 5%.

The similar values of ordered FM moments at $P = 0$ and 1.9 GPa, given in table 1 for $Pr_{0.5}Sr_{0.5}MnO_3$ at 200 K, suggest that the high pressure does not affect much the ferromagnetic Curie temperature $T_C \sim 265$ K. On the other hand, the Néel temperature T_N corresponding to the onset of the A-type AFM state with the orthorhombic structure increases markedly from 175 to about 230 K as one may conclude from the temperature dependence of the summed intensity in the two antiferromagnetic peaks (102)/(120) of the orthorhombic $Fmmm$ structure, shown as squares in figure 4. It was analysed using the experimental temperature

Table 1. Structural parameters of $Pr_{1-x}Sr_xMnO_3$ manganites ($x = 0.56$, 0.5) at different pressures and temperatures. In the tetragonal phase (space group $I4/mcm$) the atomic positions are: Pr/Sr—4(b) (0, 0.5, 0.25), Mn—4(c) (0, 0, 0), O1—4(a) (0, 0, 0.25), O2—8(h) (x, $1/2 + x$, 0). In the orthorhombic phase (space group $Fmmm$) the atomic positions are: Pr/Sr—8(h) (0, y, 0), Mn—8(d) (0.25, 0, 0.25), O1—8(g) (x, 0, 0), O2—8(i) (0, 0, z), O3—(0.25, 0.25, 0.25). For $Pr_{0.44}Sr_{0.56}MnO_3$ the values of the Mn magnetic moments for the A-type orthorhombic and C-type tetragonal AFM states obtained at $T = 16$ K are listed. For $Pr_{0.5}Sr_{0.5}MnO_3$ the values of the Mn magnetic moments for the A-type orthorhombic (at $T = 200$ and 16 K) and the FM tetragonal state at $T = 200$ K are presented.

$Pr_{0.44}Sr_{0.56}MnO_3$								
P (GPa)	0		1.9			4.8		
T (K)	290	16	290	16		290	16	
Sp. gr.	$I4/mcm$	$Fmmm$	$I4/mcm$	$Fmmm$ (77%)	$I4/mcm$ (23%)	$I4/mcm$	$Fmmm$ (70%)	$I4/mcm$ (30%)
a (Å)	5.400(3)	7.531(5)	5.393(5)	7.494(7)	5.345(8)	5.351(5)	7.465(7)	5.326(8)
b (Å)	5.400(3)	7.834(5)	5.393(5)	7.821(7)	5.345(8)	5.351(5)	7.787(7)	5.326(8)
c (Å)	7.804(5)	7.699(5)	7.778(7)	7.661(7)	7.85(1)	7.748(7)	7.614(7)	7.82(1)
Pr/Sr: y	0	0.250(2)	0	0.250(5)	0	0	0.245(5)	0
O1: x	0	0.216(2)	0	0.221(3)	0	0	0.217(4)	0
O2: x	0.783(3)	0	0.783(5)	0	0.781(7)	0.781(5)	0	0.782(7)
y	0.283(3)	0	0.283(5)	0	0.281(7)	0.281(5)	0	0.282(7)
z	0	0.286(3)	0	0.292(4)	0	0	0.290(5)	0
μ_{AFM} (μ_B)	—	$\mu_y = 3.1(1)$	—	$\mu_y = 3.1(1)$	$\mu_z = 2.0(1)$	—	$\mu_y = 3.1(1)$	$\mu_z = 2.1(1)$
R_p (%)	8.1	9.9	10.0	9.4		8.8	15.2	
R_{wp} (%)	6.3	8.6	6.3	10.0		8.9	13.2	
$Pr_{0.5}Sr_{0.5}MnO_3$								
P (GPa)	0		1.9			3.2		
T (K)	290	16	290	16		290	16	
Sp. gr.	$I4/mcm$	$Fmmm$	$I4/mcm$	$Fmmm$ (80%)	$I4/mcm$ (20%)	$I4/mcm$	$Fmmm$ (80%)	$I4/mcm$ (20%)
a (Å)	5.407(3)	7.535(5)	5.383(5)	7.490(7)	5.360(8)	5.369(5)	7.458(7)	5.337(8)
b (Å)	5.407(3)	7.838(5)	5.383(5)	7.804(7)	5.360(8)	5.369(5)	7.791(7)	5.337(8)
c (Å)	7.797(5)	7.714(5)	7.770(7)	7.654(7)	7.84(1)	7.757(7)	7.644(7)	7.80(1)
Pr/Sr: x	0	0.251(2)	0	0.262(5)	0	0	0.268(5)	0
O1: x	0	0.214(2)	0	0.214(3)	0	0	0.211(4)	0
O2: x	0.787(3)	0	0.786(5)	0	0.775(7)	0.786(5)	0	0.777(7)
y	0.287(3)	0	0.286(5)	0	0.275(7)	0.286(5)	0	0.277(7)
z	0	0.291(3)	0	0.295(4)	0	0	0.293(4)	
μ_{AFM} (μ_B)	—	$\mu_y = 3.2(1)$		$\mu_y = 3.1(1)$	—	—	$\mu_y = 3.2(1)$	—
μ_{FM} (μ_B)	$\mu_z = 2.4(1)$ (at 200 K)		$\mu_z = 2.2(1)$ (at 200 K)	—	—	$\mu_z = 2.4(1)$ (at 200 K)	—	—
R_p (%)	8.6	8.7	9.1	9.6		11.1	13.6	
R_{wp} (%)	6.6	12.1	8.5	9.9		10.4	10.8	

dependence of the Mn magnetic moment determined in detail at ambient pressure in [14]. Its application is a rather crude estimation since the observed diffraction intensity also involves the temperature variation of the AFM fraction. Nevertheless, the deduced value $T_N = 230(10)$ K at $P = 1.9$ GPa is in a very good agreement with extrapolation of the T_N versus P experimental

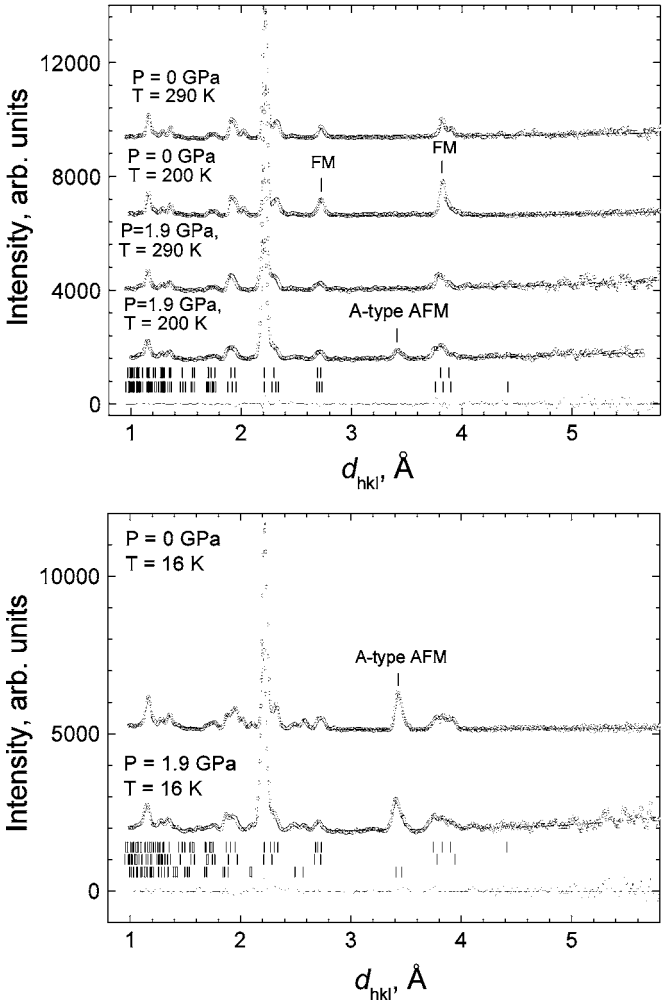

Figure 3. Neutron diffraction patterns of $Pr_{0.5}Sr_{0.5}MnO_3$ measured at $P = 0$ and 1.9 GPa, $T = 290$, 200 and 16 K at scattering angle $2\theta = 90°$ and processed by the Rietveld method. The experimental points, calculated profile and difference curve (for $P = 1.9$ GPa, $T = 290$ and 16 K) are shown. Ticks represent the calculated positions of the nuclear peaks of the $I4/mcm$ tetragonal (upper row) and $Fmmm$ orthorhombic (lower row) phases in the upper panel and positions of the nuclear (upper row) and magnetic (lower row) peaks of the $Fmmm$ orthorhombic A-type AFM phase and nuclear peaks (middle row) of the $I4/mcm$ tetragonal phase in the lower panel.

data in the 0–1.4 GPa range, recently reported for $Pr_{0.5}Sr_{0.5}MnO_3$ in [16]. Tetragonal FM and orthorhombic A-type AFM phases thus coexist below $T = 230$ K and their magnetic order develops with decreasing temperature. The analysis of nuclear peaks (110)/(002) ($I4/mcm$) + (200)/(020)/(002) ($Fmmm$) intensity (figure 4) shows, however, that the FM contribution from the tetragonal phase starts to decrease below ∼150 K and practically vanishes for $T < 60$ K, presumably with the formation of the more distorted tetragonal phase without long range magnetic order.

The complete structural data relevant to the orthorhombic and tetragonal phases of $Pr_{0.44}Sr_{0.56}MnO_3$ and $Pr_{0.5}Sr_{0.5}MnO_3$ at different pressures and temperatures are

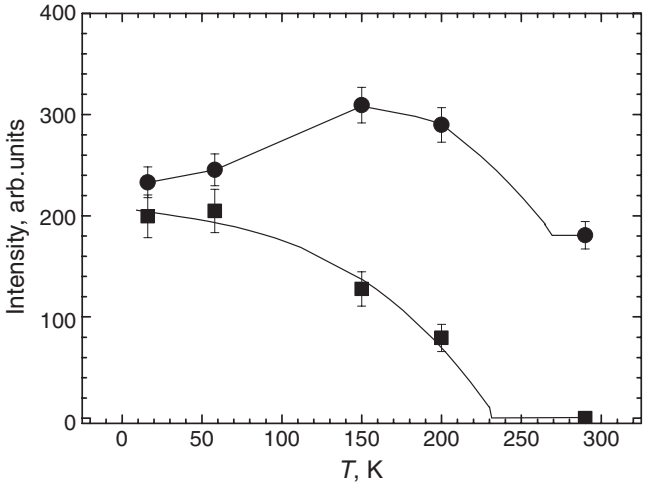

Figure 4. Temperature evolution of the magnetic order in $Pr_{0.5}Sr_{0.5}MnO_3$ at $P = 1.9$ GPa as illustrated by the temperature dependence of the combined intensity of two antiferromagnetic peaks shown as squares ((102)/(120) from the $Fmmm$ orthorhombic structure) and the temperature dependence of the combined intensity of groups of ferromagnetic and/or nuclear peaks shown as circles ((110)/(002) from the $I4/mcm$ tetragonal structure and (102)/(120) from the $Fmmm$ orthorhombic structure). The solid curves represent the suggested temperature dependence (see the text).

summarized in table 1. The tetragonal phases for both compounds reveal anisotropic compression at ambient temperature. The calculated linear compressibility $k_i = (1/a_{i0})(\mathrm{d}a_i/\mathrm{d}P)_T$ $(a_i = a, c)$ values for the c lattice parameter, $k_c = 0.0014$ and $0.0016\,\mathrm{GPa}^{-1}$, are nearly 1.4 times smaller than corresponding values for the a lattice parameter—$k_a = 0.0020$ and $0.0022\ \mathrm{GPa}^{-1}$ for $Pr_{0.44}Sr_{0.56}MnO_3$ and $Pr_{0.5}Sr_{0.5}MnO_3$, respectively. A tetragonal deformation of the lattice causes $c/a\sqrt{2}$ to increase from 1.022 to 1.024 in $Pr_{0.44}Sr_{0.56}MnO_3$ with the pressure increase up to 4.8 GPa and from 1.020 to 1.022 in $Pr_{0.5}Sr_{0.5}MnO_3$ with the pressure increase up to 3.2 GPa. As a result, an additional apical elongation of MnO_6 octahedra along the c-axis under high pressure occurs. With increase of pressure the Mn–O2 bond lengths lying in the (ab) plane decrease more rapidly in comparison with Mn–O1 bond lengths oriented along the c-axis (figure 5). Their ratio $t = l_{\mathrm{Mn-O1}}/l_{\mathrm{Mn-O2}}$ characterizing the tetragonal deformation of MnO_6 octahedra increases from $t = 1.013$ to 1.016 in $Pr_{0.44}Sr_{0.56}MnO_3$ with the pressure increase up to 4.8 GPa and from $t = 1.008$ to 1.011 in $Pr_{0.5}Sr_{0.5}MnO_3$ with the pressure increase up to 3.2 GPa. The Mn–O2–Mn bond angle increases with the pressure increase (figure 6) in both compounds and Mn–O1–Mn is equal to 180° for the $I4/mcm$ tetragonal symmetry.

At high pressure the temperature decrease leads to an increase of the tetragonal deformation of the lattice and additional elongation of MnO_6 octahedra along the c-axis occurs. In $Pr_{0.44}Sr_{0.56}MnO_3$ at $P = 4.8$ GPa the lattice parameter ratio $c/a\sqrt{2}$ increases from 1.020 ($T = 290$ K) to 1.038 ($T = 16$ K) and the tetragonal deformation of the MnO_6 octahedra increases from $t = 1.016$ ($T = 290$ K) to 1.029 ($T = 16$ K). In $Pr_{0.5}Sr_{0.5}MnO_3$ at $P = 3.2$ GPa the $c/a\sqrt{2}$ ratio increases from 1.022 ($T = 290$ K) to 1.034 and the tetragonal deformation of the MnO_6 octahedra increases from $t = 1.011$ ($T = 290$ K) to 1.026 ($T = 16$ K).

The compression of the low temperature orthorhombic phase for $Pr_{0.44}Sr_{0.56}MnO_3$ and $Pr_{0.5}Sr_{0.5}MnO_3$ is also anisotropic. The linear compressibilities of the lattice parameters at

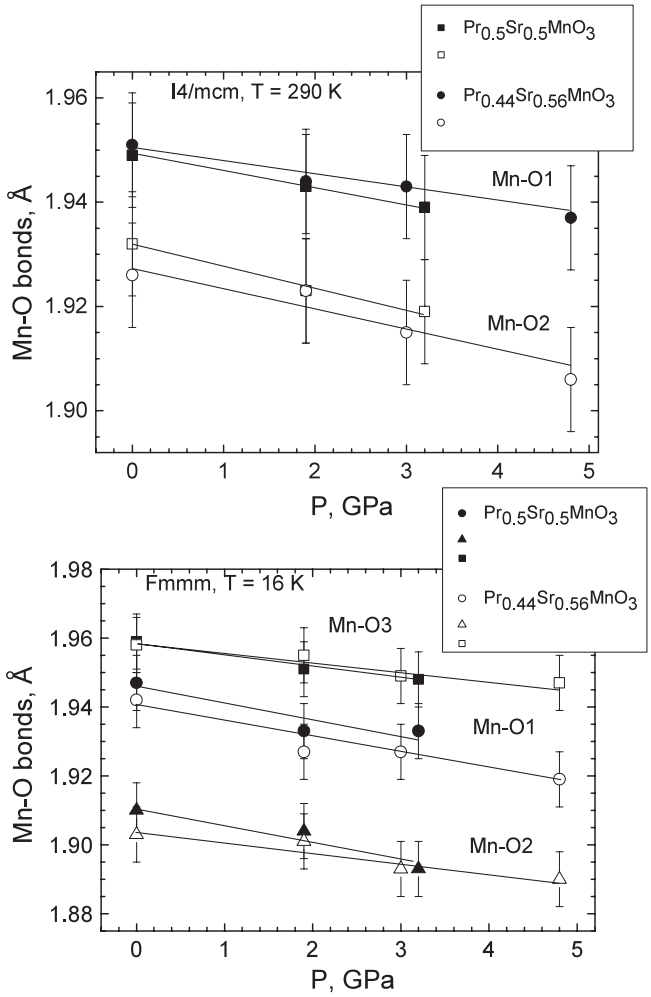

Figure 5. Mn–O bond lengths in $I4/mcm$ tetragonal (top) and $Fmmm$ orthorhombic (bottom) phases of $Pr_{0.44}Sr_{0.56}MnO_3$ and $Pr_{0.5}Sr_{0.5}MnO_3$ as functions of pressure at ambient temperature. Solid lines represent linear fits to the experimental data.

$T = 16$ K are $k_a = 0.0018$, $k_b = 0.0014$ and $k_c = 0.0023$ GPa^{-1} for $Pr_{0.44}Sr_{0.56}MnO_3$ and $k_a = 0.0028$, $k_b = 0.0019$ and $k_c = 0.0032$ GPa^{-1} for $Pr_{0.5}Sr_{0.5}MnO_3$. In the orthorhombic structure with the $Fmmm$ symmetry there are three different pairs of Mn–O bonds oriented along the crystallographic a-, b- and c-axes [14]. Between them, Mn–O1 and Mn–O3 bond lengths lying in (bc) planes have rather close values (the difference between them at $P = 0$ and $T = 16$ K is less than 1%) and the Mn–O2 bond length oriented along the a-axis is noticeably shorter (figure 5). As a result, MnO_6 octahedra in the orthorhombic phase are apically compressed along the a-axis. The value of the pseudo-tetragonal deformation of MnO_6 octahedra $t_p = 2l_{Mn-O2}/(l_{Mn-O1} + l_{Mn-O3})$ increases from 0.976 to 0.978 with the pressure increase up to 4.8 GPa in $Pr_{0.44}Sr_{0.56}MnO_3$ and remains nearly constant $t_p = 0.977$ in $Pr_{0.5}Sr_{0.5}MnO_3$.

The average of the Mn–O1–Mn and Mn–O2–Mn bond angles lying in the (ac) plane decreases with pressure increase in both $Pr_{0.44}Sr_{0.56}MnO_3$ and $Pr_{0.5}Sr_{0.5}MnO_3$ (figure 6).

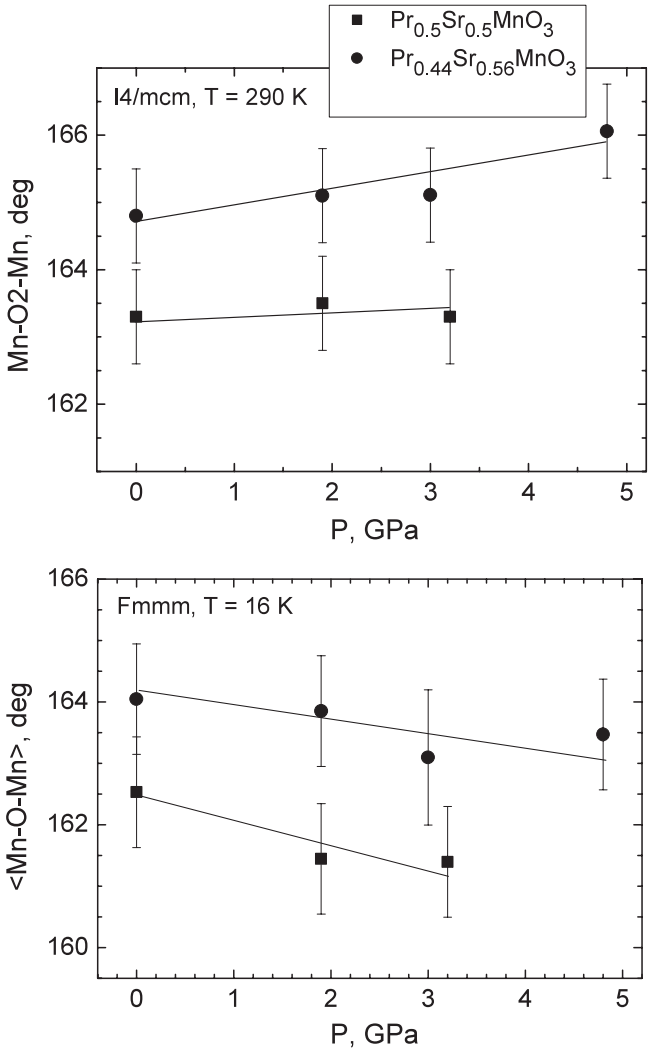

Figure 6. Top: the pressure dependence of the Mn–O2–Mn bond angle lying in the (*ab*) crystallographic plane of the $I4/mcm$ tetragonal phase of $Pr_{0.44}Sr_{0.56}MnO_3$ and $Pr_{0.5}Sr_{0.5}MnO_3$ at ambient temperature. Bottom: the pressure dependence of the average $\langle$Mn–O–Mn$\rangle$ = (Mn–O1–Mn + Mn–O2–Mn)/2 bond angle lying in the (*ac*) crystallographic plane of the orthorhombic ($Fmmm$) structure of $Pr_{0.44}Sr_{0.56}MnO_3$ and $Pr_{0.5}Sr_{0.5}MnO_3$ at $T = 16$ K. Solid lines represent linear fits to the experimental data.

The Mn–O3–Mn bond angle oriented along the *b*-axis is equal to 180° for the $Fmmm$ orthorhombic symmetry.

4. Discussion

In both $Pr_{0.44}Sr_{0.56}MnO_3$ and $Pr_{0.5}Sr_{0.5}MnO_3$ the compressibility of the lattice is smaller along the crystallographic axis corresponding to the largest lattice parameter of the structure—the *c*-axis for the tetragonal $I4/mcm$ phase and the *b*-axis for the orthorhombic $Fmmm$ phase, and the lattice is the most compressible in the plane perpendicular to this axis. In contrast to

that, calcium-doped manganites with a smaller A-site cation radius having the orthorhombic *Pnma* structure—$Pr_{0.7}Ca_{0.3}MnO_3$ [12], $La_{0.75}Ca_{0.25}MnO_3$ [21] and $La_{0.67}Ca_{0.33}MnO_3$ [11]—exhibit the opposite compression anisotropy, although the linear compressibilities of the lattice parameters of strontium and calcium-doped manganites have comparable values. In this case the lattice is most compressible along the largest *b*-axis of the *Pnma* crystal structure.

One should note that at normal pressure and intermediate temperatures both $Pr_{0.5}Sr_{0.5}MnO_3$ and $Pr_{0.44}Sr_{0.56}MnO_3$ compounds exhibit the apical elongation of the MnO_6 octahedra which is favourable for the appearance of the C-type AFM state due to the enhanced population of the $d(3z^2 - r^2)$ orbitals oriented along the *c*-axis [10]. However, at sufficiently low temperatures the onset of an A-type AFM state and the concurrent structural phase transition from the tetragonal $I4/mcm$ to the orthorhombic $Fmmm$ phase are observed. This phase transition leads to the apical compression of MnO_6 octahedra along the *a*-axis of the orthorhombic structure corresponding to the enhanced population of the $d(y^2 - z^2)$ orbitals. Such a behaviour may be explained by the higher kinetic energy gain allowed for the A-type AFM state in comparison with the C-type AFM state which makes the A-type AFM state more energetically favourable [5, 22, 23]. Indeed, the enhanced polarization of the $d(y^2-z^2)$ orbitals in the A-type AFM state allows an electron transfer within ferromagnetic planes leading to the metallic-like conductivity with a two-dimensional character [7, 13]. In contrast to that, the enhanced polarization of the $d(3z^2 - r^2)$ orbitals in the C-type AFM state allows electron transfer along *c*-axis ferromagnetic chains only and this state is insulating [23].

The application of high pressure leads to an anisotropic contraction of the perovskite lattice, which results in further increase of the $d(3z^2-r^2)$ population due to the additional apical elongation of the MnO_6 octahedra. This is a reason for some destabilization in $Pr_{0.5}Sr_{0.5}MnO_3$ of the FM state at intermediate temperatures in favour of the A-type AFM one. At lower temperatures, the residual FM regions are reversed to a more distorted tetragonal phase without magnetic order, that can be alternatively interpreted as some nanotexture of orthorhombic twins. In $Pr_{0.44}Sr_{0.56}MnO_3$ high pressure induces in the A-type ground state a minority of the true tetragonal C-type AFM state that is common otherwise for systems with larger Sr content.

There have been several theoretical attempts to construct the phase diagram of manganites $Ln_{1-x}A_xMnO_3$ for the doping level range $x > 0.5$ [5, 22, 24]. The problem of the double exchange is treated with the help of the following effective Hamiltonian in the simple cubic perovskite lattice ($a_p \times a_p \times a_p$):

$$H = J_{AF} \sum_{\langle ij \rangle} \vec{S}_i \vec{S}_j - J_H \sum_{i,\alpha,\mu,\mu'} \vec{S}_i \cdot c^{\dagger}_{i\alpha\mu} \vec{\sigma}_{\mu\mu'} c_{i\alpha\mu'} - \sum_{\langle ij \rangle,\mu} t^{\alpha\beta}_{ij} c^{\dagger}_{i\alpha\mu} c_{j\beta\mu}. \qquad (1)$$

Here the first term describes the AF superexchange interaction between the localized t_{2g} spins $\vec{S}_i$ and $\vec{S}_j$ at the nearest-neighbour sites *i* and *j*, while the second and third terms lead effectively to a FM interaction. The second term relates to the Hund coupling between the spins of itinerant e_g electrons and t_{2g} spins and the third term represents the gain of kinetic energy due to hopping of e_g electrons. These electrons are labelled by the site index i (j), orbital index α (β), corresponding to $d(3z^2 - r^2)$ and $d(x^2 - y^2)$ orbitals, and spin index μ (μ') corresponding to the e_g-electron spin +1/2 and −1/2; $\vec{\sigma}_{\mu\mu'}$ are Pauli matrices and $t^{\alpha\beta}_{ij} = t\langle i\alpha/j\beta\rangle$ are hopping matrix elements describing the intensity of the electron transfer between the nearest-neighbouring sites via oxygen p orbitals. The operator $c^{\dagger}_{i\alpha\mu}$ creates an e_g electron with a spin μ in the orbital α at site i.

The solution of the Hamiltonian gives magnetic ground states as a function of doping level x and two adjustable parameters, $J_{AF}S^2/t$ and J_HS/t. The recent calculations at fixed $J_HS/t = 5$ of Venketeswara Pai [22] show that the observed phase diagram for $Pr_{1-x}Sr_xMnO_3$ can be correctly reproduced for a value of $J_{AF}S^2/t = 0.053$ if the effects of finite e_g band

filling are taken into account. In agreement with the experiment, a sequence of FM, A-type, C-type and G-type AFM order is obtained in the $x \sim 0.5$–1 region. It is worth mentioning that the theoretical values $J_H S/t = 5$ and $J_{AF}S^2/t = 0.053$ ($S = 1.5$) are close to real ones which can be calculated using values of $J_H \approx 0.7$ eV obtained from photoemission spectroscopy data [25] and $t = 0.195$ eV and $J_{AF} = 3.3$ meV determined from the spin wave dispersion of the compound $Nd_{0.45}Sr_{0.55}MnO_3$ [26] with structural and magnetic properties similar to those of $Pr_{0.5}Sr_{0.5}MnO_3$ and $Pr_{0.44}Sr_{0.56}MnO_3$.

Further, the analysis of the model phase diagram [22] as a function of parameter $J_{AF}S^2/t$ shows that for a fixed value $J_H S/t = 5$ and the doping level $x = 0.5$, the transition from the FM to the A-type AFM state occurs at a critical value $J_{AF}S^2/t = 0.051$, and the transition from the A-type AFM to the C-type AFM state, at $J_{AF}S^2/t = 0.067$. For the doping level $x = 0.56$ and $J_H S/t = 5$ these transitions occur at slightly different values $J_{AF}S^2/t = 0.047$ and 0.057, respectively. These critical $J_{AF}S^2/t$ values can be used for a semi-quantitative analysis of the high pressure effect on the stability of the magnetic states of $Pr_{0.5}Sr_{0.5}MnO_3$ and $Pr_{0.44}Sr_{0.56}MnO_3$.

In the analysis we neglect for simplicity the pressure dependence of the $J_H S/t$ parameter as well as the variation of the Mn–O–Mn bond angles and suppose that parameters t and J_{AF} depend mainly on the average Mn–O bond length l. Considering that the hopping integral is proportional to the overlap of 3d orbitals via oxygen p orbitals and the superexchange integral varies as its fourth order [26–28], one actually finds $t \sim l^{-3.5}$ and $J_{AF} \sim l^{-14}$. The variation of the $J_{AF}S^2/t$ parameter with high pressure can thus be expressed as $J_{AF}S^2/t = (J_{AF}S^2/t)_0(l(P)/l_0)^{-10.5}$, where l_0 is the average Mn–O bond length at $P = 0$ and the ambient pressure value $(J_{AF}S^2/t)_0 = 0.053$. For $Pr_{0.44}Sr_{0.56}MnO_3$, this value falls into the predicted region of existence of the A-type AFM state, in agreement with the observation of a robust A-type AFM ground state, while for $Pr_{0.5}Sr_{0.5}MnO_3$ it appears close to boundary with the FM ground state (the theoretical critical value for the FM–A-type AFM transition $J_{AF}S^2/t = 0.051$). This may explain why $Pr_{0.5}Sr_{0.5}MnO_3$ with the A-type AFM ground state reverses to the FM state at intermediate temperatures.

The parameter $J_{AF}S^2/t$ for $Pr_{0.44}Sr_{0.56}MnO_3$ and $Pr_{0.5}Sr_{0.5}MnO_3$ calculated as a function of relative average Mn–O bond length l/l_0 is displayed in figure 7. Upon compression, the $J_{AF}S^2/t$ parameter increases and the critical value for the A-type AFM–C-type AFM transition is reached at $l/l_0 = 0.993$ ($P_{crit} \approx 3.5$ GPa) for $Pr_{0.44}Sr_{0.56}MnO_3$ and at $l/l_0 = 0.978$ ($P_{crit} \approx 10$ GPa) for $Pr_{0.5}Sr_{0.5}MnO_3$ (figure 7). The value obtained for the transition pressure P_{crit} for $Pr_{0.44}Sr_{0.56}MnO_3$ agrees satisfactorily with the observation of the C-type AFM phase in this compound at $P \approx 1.9$ GPa. The calculated value $P_{crit} \approx 10$ GPa for $Pr_{0.5}Sr_{0.5}MnO_3$ is much higher than the maximum pressure achieved in the present study and this explains why no C-type AFM order was observed in this compound.

5. Conclusions

The $Pr_{1-x}Sr_xMnO_3$ systems studied are characterized by a near degeneracy of three magnetic ground states—the FM metallic, A-type AFM metallic and C-type AFM insulating ones. Their stability can be controlled by small variations of the composition $x \sim 0.5$–0.6 (chemical stress), by the uniaxial stress due to the misfit between the substrate and sample in thin films or, in the bulk, by the applied external stress. The results of our study show that $Pr_{0.44}Sr_{0.56}MnO_3$ and $Pr_{0.5}Sr_{0.5}MnO_3$, both with the A-type AFM ground state at ambient pressure, form under high external pressure a non-uniform state in the crystallographic and magnetic sense. It consists of a mixture of the orthorhombic A-type AFM phase and the tetragonal phase which possesses C-type AFM magnetic order in $Pr_{0.44}Sr_{0.56}MnO_3$ and does not exhibit long range magnetic order

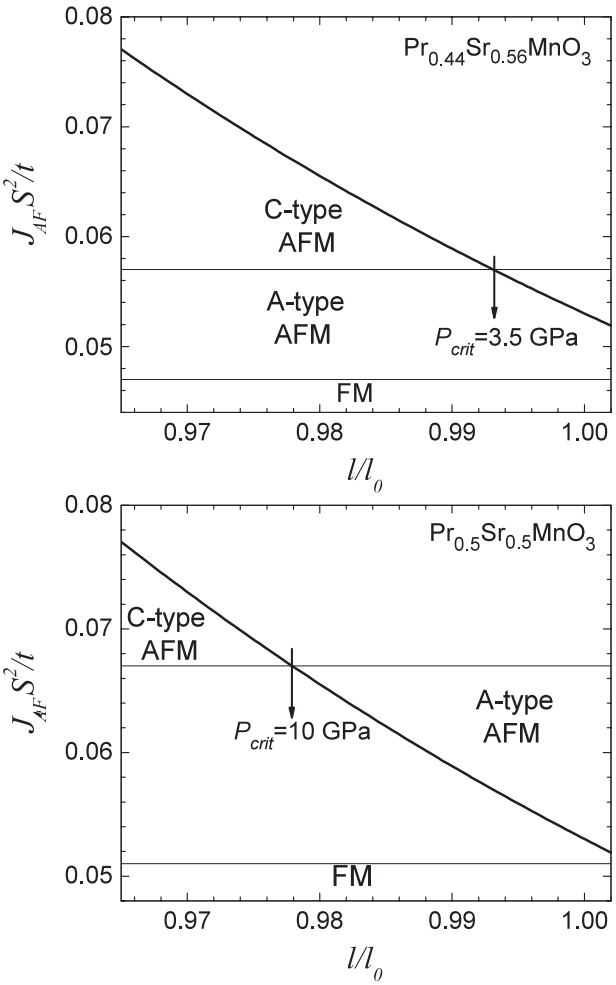

Figure 7. Parameter $J_{AF}S^2/t$ as a function of relative average Mn–O bond length l/l_0 for $Pr_{0.44}Sr_{0.56}MnO_3$ and $Pr_{0.5}Sr_{0.5}MnO_3$. The critical values $J_{AF}S^2/t$ of the model phase diagram of the manganites [22] corresponding to FM–A-type AFM and A-type–C-type AFM phase transitions in $Pr_{0.44}Sr_{0.56}MnO_3$ and $Pr_{0.5}Sr_{0.5}MnO_3$ are shown as horizontal lines. Arrows indicate the critical l/l_0 values for the A-type–C-type AFM phase transitions in $Pr_{0.44}Sr_{0.56}MnO_3$ and $Pr_{0.5}Sr_{0.5}MnO_3$.

in $Pr_{0.5}Sr_{0.5}MnO_3$. In $Pr_{0.5}Sr_{0.5}MnO_3$ a suppression of the temperature interval of existence of the intermediate FM state also occurs under high pressure.

The stabilization of the C-type AFM state in $Pr_{0.44}Sr_{0.56}MnO_3$ and suppression of the intermediate isotropic three-dimensional FM state in $Pr_{0.5}Sr_{0.5}MnO_3$ can be related to two effects of high pressure. The first one is compression anisotropy of the perovskite lattice. This leads to the noticeable apical elongation of MnO_6 octahedra under high pressure in the tetragonal phase and creates the enhanced $d(3z^2 - r^2)$ orbital polarization, favourable for the C-type AFM order, observed in $Pr_{0.44}Sr_{0.56}MnO_3$. The second, probably more important effect is the contraction itself. A semi-quantitative analysis of this effect is based on the fact that AFM superexchange and FM double-exchange interactions increase with decreasing Mn–O lengths according to different power laws. Using the model phase diagram obtained

in terms of parameters $J_{AF}S^2/t$ and $J_H S/t$ which reflect the strength of the superexchange, Hund coupling and electron transfer in manganites, the critical pressure for the A-type AFM–C-type AFM phase transition is calculated to be $P_{crit} \approx 3.5$ GPa for $Pr_{0.44}Sr_{0.56}MnO_3$, in satisfactory agreement with the experimental observation of this work and $P_{crit} \approx 10$ GPa in $Pr_{0.5}Sr_{0.5}MnO_3$. One could thus expect the appearance of the C-type AFM state in the latter compound at higher pressures than are at present available.

Acknowledgments

The work was supported by the Russian Foundation for Basic Research, grant 03-02-16879, and the Russian Ministry of Science, Industry and Technology, state contract No 40.012.1.1.1148, and a grant of support for unique facilities of Russia.

References

[1] Dagotto E, Hotta T and Moreo A 2001 *Phys. Rep.* **344** 1
[2] Zener C 1951 *Phys. Rev.* **82** 403
[3] Anderson P W and Hasegawa H 1955 *Phys. Rev.* **100** 675
[4] De Gennes P-G 1960 *Phys. Rev.* **118** 141
[5] Maezono R, Ishihara I and Nagaosa N 1998 *Phys. Rev.* B **58** 11583
[6] Chmaissem O, Dabrowski B, Kolesnik S, Mais J, Jorgensen J D and Short S 2003 *Phys. Rev.* B **67** 094431
[7] Pollert E, Jirák Z, Hejtmánek J, Strejc A, Kužel R and Hardy V 2002 *J. Magn. Magn. Mater.* **246** 290
[8] Kajimoto R, Yoshizawa Y, Kawano H, Tokura Y, Ohoyama K and Ohashi M 1999 *Phys. Rev.* B **60** 9506
[9] Konishi Y *et al* 1999 *J. Phys. Soc. Japan* **68** 3790
[10] Fang Z, Solovyev I V and Terakura K 2000 *Phys. Rev. Lett.* **84** 3169
[11] Kozlenko D P, Glazkov V P, Sadykov R A, Savenko B N, Voronin V I and Medvedeva I V 2003 *J. Magn. Magn. Mater.* **258/259** 290
[12] Kozlenko D P, Glazkov V P, Medvedeva I V, Savenko B N and Voronin V I 2003 *High Pressure Res.* **23** 149
[13] Kozlenko D P, Glazkov V P, Jirák Z and Savenko B N 2003 *J. Magn. Magn. Mater.* **267** 120
[14] Damay F, Martin C, Hervieu M, Maignan A, Raveau B, André G and Boureé F 1998 *J. Magn. Magn. Mater.* **184** 71
[15] Hejtmánek J, Pollert E, Jirák Z, Sedmidubský D, Strejc A, Maignan A, Martin Ch, Hardy V, Kužel R and Tomioka Y 2002 *Phys. Rev.* B **66** 014426
[16] Medvedeva I, Martin C, Bersenev Yu, Morchshakov V, Bärner K and Raveau B 2004 *Phys. Met. Metallogr.* **97** 169
[17] Aksenov V L, Balagurov A M, Glazkov V P, Kozlenko D P, Naumov I V, Savenko B N, Sheptyakov D V, Somenkov V A, Bulkin A P, Kudryashev V A and Trounov V A 1999 *Physica* B **265** 258
[18] Glazkov V P and Goncharenko I N 1991 *Fiz. Tekh. Vysokih Davlenij* **1** 56 (in Russian)
[19] Zlokazov V B and Chernyshev V V 1992 *J. Appl. Crystallogr.* **25** 447
[20] Rodriguez-Carvajal J 1993 *Physica* B **192** 55
[21] Meneghini C, Levy D, Mobilio S, Ortolani M, Nuñez-Reguero M, Kumar A and Sarma D D 2001 *Phys. Rev.* B **65** 012111
[22] Venketeswara Pai G 2001 *Phys. Rev.* B **63** 064431
[23] Xu Sh, Moritomo Y, Machida A, Ohoyama K, Kato K and Nakamura A 2002 *Phys. Rev.* B **66** 024420
[24] Van der Brink J and Khomskii D 1999 *Phys. Rev. Lett.* **82** 1016
[25] Oleś A M and Feiner L F 2002 *Phys. Rev.* B **65** 052414
[26] Jackeli G, Perkins N B and Plakida N M 2001 *Phys. Rev.* B **64** 092403
[27] Harrison W A 1980 *The Electronic Structure and Properties of Solids* (San Francisco, CA: Freeman)
[28] Zhou J-S and Goodenough J B 2003 *Phys. Rev.* B **68** 054403